Journal of Materials Chemistry A

ROYAL SOCIETY OF CHEMISTRY

PAPER

View Article Online
View Journal | View Issue

Cite this: J. Mater. Chem. A, 2022, 10, 9997

Oil foams stabilized by POSS/organosilica particle assemblies: application for aerobic oxidation of aromatic alcohols†

Shi Zhang,[ab] Dmytro Dedovets[b] and Marc Pera-Titus *[ac]

A novel amphiphilic polyhedral oligomeric silsesquioxane (POSS) with surfactant-like behavior was synthesized. By combining this new POSS, used as a frother, with surface-active catalytic organosilica particles, used as a stabilizer, we designed a dual particle system able to generate foams in pure organic solvents. Tunable foamability and foam stability were achieved in a variety of organic solvents by simply adjusting the POSS concentration. As a result, the catalytic activity was drastically boosted in the aerobic oxidation of pure aromatic alcohols under 1 bar O_2 pressure. Particles were conveniently recycled with high foamability and the catalytic efficiency was maintained for at least 7 consecutive runs.

Received 24th January 2022
Accepted 17th March 2022

DOI: 10.1039/d2ta00667g

rsc.li/materials-a

1. Introduction

Foams are widely used in industrial applications such as food manufacturing processes, cosmetics, healthcare products, fire extinguishing, wastewater treatment (froth flotation), and enhanced oil recovery.[1–4] Recently, foams have been formulated for more elaborate applications such as the manufacture of porous materials[5] and catalysis.[6] Particle-stabilized (or Pickering) foams are often more attractive compared to surfactant-based counterparts due to their much higher stability under harsh conditions (*e.g.*, shear stress and high temperature). Particle-stabilized aqueous foams have been thoroughly studied using a variety of stabilizers such as polymers,[7] proteins,[8] particles[9] and crystals.[10] However, few studies have focused on non-aqueous/oil foams owing to the low surface tension of organic solvents, restricting particle adsorption at the gas–liquid interface. Nonetheless, there is room to design particle-stabilized non-aqueous/oil foams for gas-liquid-solid microreactors comprising water-insoluble reactants.

The formation of foams depends on three main factors. First, the particles need to be dispersed in the solvent and agglomeration should be limited. Second, stable foams can be generated only if the interfacial contact angle of particles lies in the "stability window" range. Contrary to Pickering emulsions, the range of contact angles for foam formation is much narrower,[11] making the design of surface-active particles challenging and with limited scope for accessible organic solvents. Third, owing to the much larger size of particles compared to surfactants, the kinetics of particle adsorption at the gas–liquid interface is notably slower, leaving enough time for bubble coalescence before sufficient surface coverage by particles can be achieved. Overall, ideal particles that promote foamability and foam stability should be highly dispersible in the solvent, exhibit an interfacial contact angle in the "stability window" range, and display fast adsorption kinetics. Nonetheless, particles meeting all these requirements simultaneously for a given solvent are scarce. In practice, particle-stabilized foams are often prepared using co-solvents[12] or surfactants,[13,14] to tune the particle dispersion and interfacial contact angle. The use of co-solvents, however, complicates further product separation and purification steps, whereas the use of surfactants is limited to aqueous foams only,[15] as particle–surfactant interactions are driven by hydrophobic forces not existing in organic systems. Moreover, separation and purification in the case of surfactants is not straightforward.

Here we designed a dual particle system for foam stabilization in a broad range of organic reagents, and engineered efficient gas–liquid–solid multiphase microreactors for the aerobic oxidation of alcohols. The system combines surface-active oleophobic (fluorinated) silica particles incorporating Pd nanoparticles, used as stabilizers, and fluorinated anisotropic polyhedral oligomeric silsesquioxanes (POSSs), used as frothers. POSS are very small silica nanoparticles with surfactant-like behavior.[16,17] They can stabilize foams and tune the wettability of large particles similarly to silica/surfactant mixtures in aqueous systems. Unlike surfactants, POSS can be separated by simply adjusting the liquid composition. POSS are also good candidates for catalytic applications owing to their thermal[18] and chemical stability.[19–21]

[a]Efficient Products and Processes Laboratory (E2P2L), UMI 3464 CNRS-Solvay, 3966 Jin Du Road, Xin Zhuang Ind Zone, 201108 Shanghai, China. E-mail: marc.pera-titus-ext@solvay.com

[b]Laboratoire du Futur (LOF), UMR 5258 CNRS-Solvay-Universite Bordeaux 1, 178 Av Dr Albert Schweitzer, 33608 Pessac Cedex, France

[c]Cardiff Catalysis Institute, School of Chemistry, Cardiff University, Main Building, Park Place, Cardiff CF10 3AT, UK. E-mail: peratitusm@cardiff.ac.uk

† Electronic supplementary information (ESI) available. See DOI: 10.1039/d2ta00667g

2. Results and discussion

2.1. Preparation of surface-active POSS particles

Phenyl-based POSS (*i.e.* Ph_7-POSS) was synthesized by hydrolytic condensation of triethoxylphenylsilane under basic conditions (Fig. 1a) (see the ESI† for experimental details).[22] The sample was further functionalized with fluorinated chains by reaction with trichloro(1*H*,1*H*,2*H*,2*H*-perfluorooctyl)silane (*i.e.* Ph_7/F_{13}-POSS), allowing corner-capping of Si–ONa groups. The ^{29}Si NMR MAS spectrum of Ph_7/F_{13}-POSS (Fig. 1b) exhibits two bands at −68.7 and −78.6 ppm. These bands appear within the T3 range and evidence the closure of the POSS cage after the corner-capping reaction.[23,24] The Si atom bound directly to the benzene ring has a lower chemical shift due to the higher electron density of phenyl groups.[25] The ^{13}C NMR MAS spectra of the samples before and after capping (Fig. S1†) show a complex band in the range of 125–138 ppm belonging to aromatic groups.[26] Two additional bands are visible at 2.5 and 25 ppm in Ph_7/F_{13}-POSS that can be assigned to CH_2 groups in fluorinated chains.[27] Besides, a broad and complex band appears in the range of 110–120 ppm that can be assigned to CF_3 and CF_2 groups in fluorinated chains.[28] Tetrahydrofuran (THF), which was used as solvent for Ph_7-POSS synthesis, is visible in the corresponding spectrum.[27] This band vanishes after grafting the fluorinated chains, pointing out the full capping of all Si–ONa groups in Ph_7-POSS. The ^{19}F NMR MAS spectrum of Ph_7/F_{13}-POSS displays a sharp signal at 80.7 ppm that can be ascribed to CF_3 groups (Fig. S2†).[28] Additional sharp bands are visible in the range of 115–128 ppm that can be ascribed to internal CF_2 groups.[28]

Ph_7-POSS and Ph_7/F_{13}-POSS were also analyzed by FT-IR spectroscopy (Fig. 1c). Typical bands of silica appear at 1100 cm^{-1} and 800 cm^{-1} that can be assigned to asymmetric stretching and bending vibrations of Si–O–Si bonds, respectively.[29] A broad band appears in the range of 3000–3500 cm^{-1} for Ph_7-POSS belonging to Si–ONa groups interacting with adsorbed water. This band vanishes for Ph_7/F_{13}-POSS, which confirms the capping of Si–ONa groups. Characteristic bands ascribed to the fluorocarbon chain appear at 913, 1171 and 1237 cm^{-1} that can be assigned to stretching modes of C–Si and C–F (CF_2/CF_3) bonds, respectively.[29] Additional bands at 710 and 670 cm^{-1} are attributed to the symmetric stretching bands of CF_3 groups.[30] Bands ascribed to the aromatic skeleton appear at 3100 cm^{-1} for asymmetric stretching modes of C–H groups, and at 1620 cm^{-1}, 1430 cm^{-1} and 750 cm^{-1}, that can be attributed to C–H stretching and in-place and out-plane bending vibrations, respectively.[31] Additional overtones ascribed to aromatic groups appear in the range of 1750–2000 cm^{-1}.[31]

TG analysis was used to explore the thermal stability of Ph_7-POSS and Ph_7/F_{13}-POSS (Fig. 1d). Ph_7-POSS exhibits a small weight loss until 100 °C (about 5%) that is attributed to water desorption. Phenyl groups start to decompose at 380 °C with a weight loss of about 37% matching the theoretical value (38.4%). After corner-capping of –ONa groups, Ph_7/F_{13}-POSS shows almost no weight loss below 400 °C, but has a higher overall weight loss as compared to Ph_7-POSS, up to 600 °C.

The XRD pattern of Ph_7/F_{13}-POSS (Fig. S3†) exhibits two diffraction bands at 2θ values of *ca.* 8.3° and 18.9° corresponding to a *d*-spacing of *ca.* 11 and 5 Å, respectively, that can be attributed to the overall dimension and body diagonal of the POSS cage, respectively.[32] The sample shows a semicrystalline nature which is known to be related to the choice of solvent and lattice stabilization conditions.[27]

The elementary particle size and aggregation behavior of Ph_7/F_{13}-POSS was inspected in different solvents by dynamic light scattering (DLS). In toluene and THF (Fig. S4a and b†), which are good solvents for POSS with phenyl groups,[33] the average particle size is below 10 nm at low POSS concentration (≤0.1 wt%). This value is in line with the theoretical particle size of Ph_7/F_{13}-POSS (1–3 nm),[34] with only partial aggregation. However, at a Ph_7/F_{13}-POSS concentration above 0.3 wt%, large aggregates are observed in toluene. In contrast, in benzyl

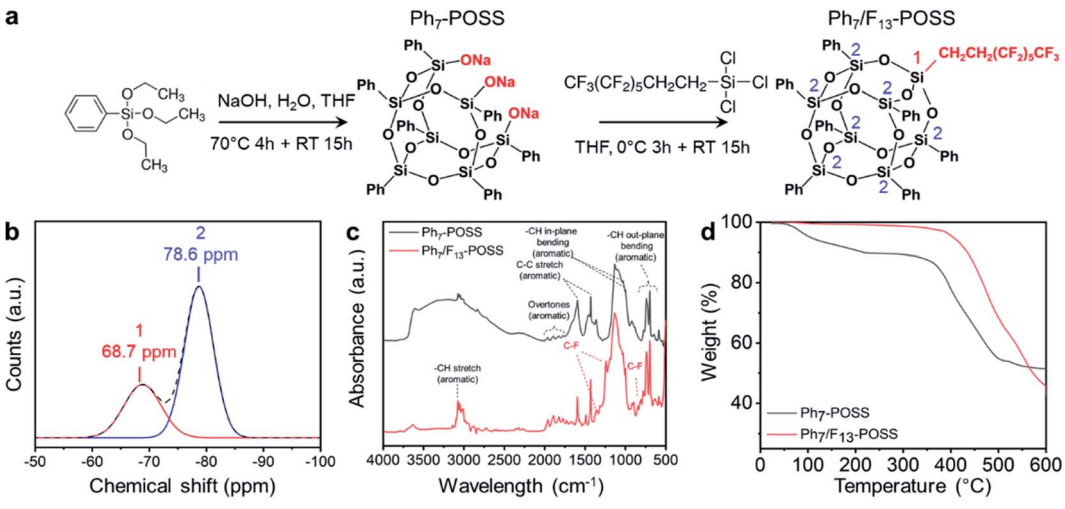

Fig. 1 (a) Synthesis of Ph_7/F_{13}-POSS. (b) ^{29}Si NMR MAS spectra of Ph_7/F_{13}-POSS. (c) FT-IR of Ph_7-POSS and Ph_7/F_{13}-POSS. (d) TGA of Ph_7-POSS and Ph_7/F_{13}-POSS.

alcohol (Fig. S4c†), Ph_7/F_{13}-POSS is present as aggregates even at extremely low concentration (0.001 wt%).

2.2. Foamability of Ph_7/F_{13}-POSS

The foamability of Ph_7/F_{13}-POSS was tested in benzyl alcohol (BnOH), anisole and toluene, with a surface tension of 39, 35 and 28.4 mN m^{-1} at 20 °C, respectively. In all cases, foams are generated after handshaking of a 2 mL sample (Fig. 2a), and the foam height increases with the particle concentration (Fig. 2b). In benzyl alcohol, foams are stable for at least 30 min above 0.3 wt% Ph_7/F_{13}-POSS, whereas they destabilize within 1 min in anisole and toluene (Fig. 2c). The foam volume increases with the Ph_7/F_{13}-POSS concentration, but the foam stability does not improve (Fig. S5†), which may be explained by the low adsorption energy of Ph_7/F_{13}-POSS due to its small particle size. We extended our analysis to 39 other liquids (Table S1†) to assess the foaming scope of Ph_7/F_{13}-POSS (Fig. S6†). Ph_7/F_{13}-POSS can generate foams provided that the surface tension of the liquid is higher than 27 mN m^{-1}. No foams are produced in very polar liquids (diols and polyols, surface tension ≥45 mN m^{-1}) due to the poor dispersion of Ph_7/F_{13}-POSS.

Particle adsorption at gas–liquid and liquid–liquid interfaces is often regarded to have no or marginal effect on the surface tension.[14,35,36] However, POSS materials were shown to exhibit interfacial activity similar to surfactants.[37] To assess the surface activity of Ph_7/F_{13}-POSS at the gas–liquid interface, we measured the surface tension of benzyl alcohol at variable Ph_7/F_{13}-POSS concentrationusing the maximum bubble pressure method (Fig. 2d).[38] The surface tension of pure benzyl alcohol is 39.6 mN m^{-1}. Upon dispersing 0.1 wt% Ph_7/F_{13}-POSS, the surface tension decreases to 30 mN m^{-1}, and declines further to 27 mN m^{-1} at 0.5 wt% concentration. The surface tension drops fast for a surface age within 50 000 ms. Beyond this value, it decreases smoothly due to continuous interfacial particle adsorption, and remains almost unchanged above 160 000 ms, especially at a POSS concentration above 0.4 wt%.

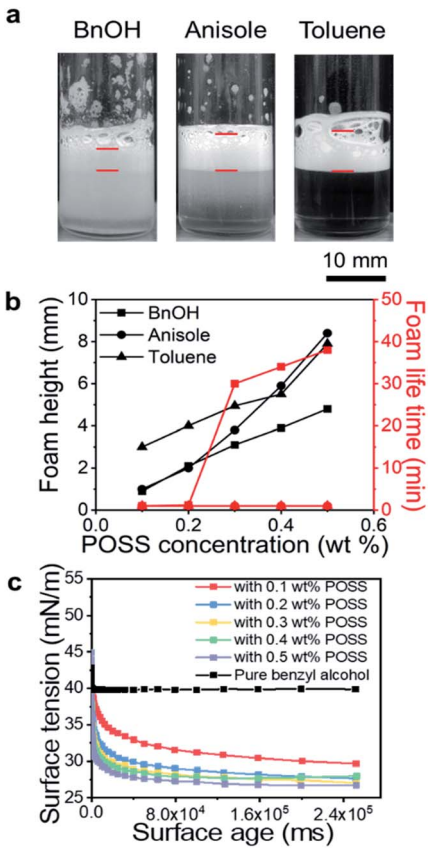

Fig. 2 (a) Macroscopic image of foams in benzyl alcohol, anisole and toluene stabilized by 0.5 wt% Ph_7/F_{13}-POSS in 2 mL of liquid. (b) Effect of the Ph_7/F_{13}-POSS concentration on the foam height at time = 0, and foam lifetime. (c) Dynamic surface tension of benzyl alcohol at variable Ph_7/F_{13}-POSS concentrations.

2.3. Foamability of Ph_7/F_{13}-POSS/fluorinated silica particle mixtures

We showed above that Ph_7/F_{13}-POSS nanoparticles exhibit surface-active behavior at the gas–liquid interface. However, except for benzyl alcohol, the stability of foams is poor. To promote foam stability, we combined Ph_7/F_{13}-POSS with larger oleophobic particles, which can irreversibly adsorb at the gas–liquid interface. A fluorinated organosilica (33 wt% F, 364 nm particle size) was synthesized by the Stöber method using *1H*,*1H*,*2H*,*2H*-perfluorodecyltriethoxysilane (PFDTES), 3-mercaptopropyltriethoxysilane (MPTES) and tetraethyl-orthosilicate (TEOS) precursors, with TEOS/MPTES and TEOS/PFDTES molar ratios of 16 and 4, respectively (see the ESI† for details). Catalytic Pd nanoparticles were further loaded by wet impregnation using an ethanolic solution of $Pd(OAc)_2$.The final particles were denoted as Pd@SiNP_F_{17} (1.33 wt% Pd).

The foaming properties of Ph_7/F_{13}-POSS and Pd@ SiNP_F_{17} mixtures were first tested in benzyl alcohol using 0.1 wt% Ph_7/F_{13}-POSS and 2 wt% Pd@SiNP_F_{17} (Fig. 3a and S7†). Pd@SiNP_F_{17} alone, with a contact angle of 95° (Fig. S8†), is poorly dispersible at room temperature, and only some bubbles are generated. In parallel, Ph_7/F_{13}-POSS alone can make foams (contact angle of 58°, Fig. S9†), but their stability at 0.1 wt% is limited to 3 min. When both particles are combined, small amounts of Ph_7/F_{13}-POSS helps Pd@SiNP_F_{17} to disperse (see DLS distributions in Fig. S10a†), resulting in modest foaming with a layer of bubbles remaining for 20 min. Increasing the Ph_7/F_{13}-POSS concentration to 0.3 wt% at 2 wt% Pd@SiNP_F_{17} results in a higher foam height and 1 h stability. Further increase of the Ph_7/F_{13}-POSS concentration to 0.5 wt% results in a higher initial foam height, but with much lower stability, also encompassing lower particle dispersion.

Given these results, we extended our analysis to anisole and toluene (Fig. 3b, c, S7, S10b and c†). In analogy to BnOH, Pd@SiNP_F_{17} is poorly wetted and cannot be dispersed in both solvents, resulting in large agglomerates with an average size of about 500 nm that sediment within 2 min. In both cases, Ph_7/F_{13}-POSS alone (0.1–0.5 wt%) generates poorly stable foams, which destabilize within 2 min. With 2 wt% Pd@SiNP_F_{17} and 0.1–0.3 wt% Ph_7/F_{13}-POSS, foams are much more stable (for more than 1 h) with no obvious collapse even after several days (data not shown). Noteworthy, after adding Ph_7/F_{13}-POSS,

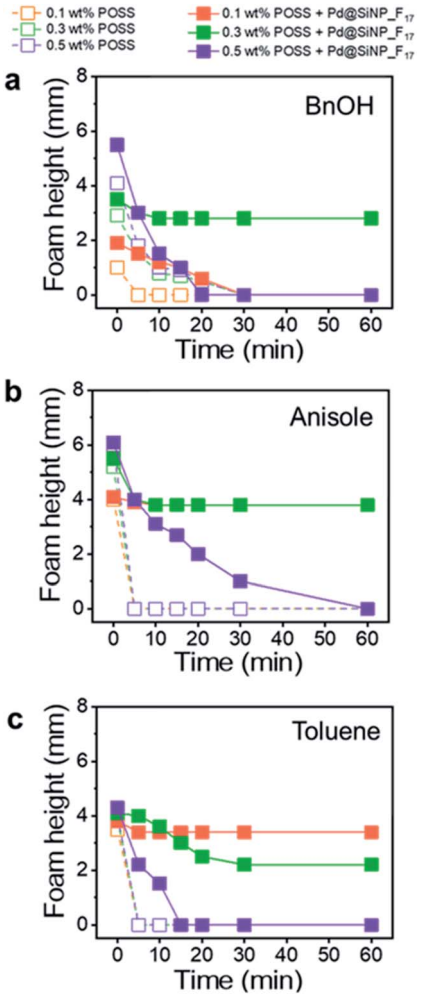

Fig. 3 Foam height at room temperature with 2 wt% Pd@SiNP_F_{17} in 2 mL of (a) benzyl alcohol, (b) anisole and (c) toluene at variable Ph_7/F_{13}-POSS concentrations.

Pd@SiNP_F_{17} can be dispersed without sedimentation after 10 min, suggesting that Pd@SiNP_F_{17} particles are surrounded by Ph_7/F_{13}-POSS, altering the wettability. The two-particle interactions are driven most likely by van der Waals forces.[39] However, the foam stability decreases down to 15 min when the Ph_7/F_{13}-POSS concentration is further increased to 0.5 wt%. At these conditions, larger agglomerates are again apparent, disfavoring dispersion. The foam stability at this high Ph_7/F_{13}-POSS concentration may be preserved by increasing the Pd@SiNP_F_{17} concentration to 4 wt% and 6 wt% (Fig. S12†). Finally, to show universality of the approach, we obtain highly stable foams in 10 additional liquids using 2 wt% Pd@SiNP_F_{17} and 0.1 wt% Ph_7/F_{13}-POSS (Fig. S13†).

To gain more insight into the interactions between Ph_7/F_{13}-POSS and Pd@SiNP_F_{17} particles, we surveyed the effect of Ph_7/F_{13}-POSS on the surface tension of benzyl alcohol in the presence of Pd@SiNP_F_{17} (Fig. 4a). At a low Ph_7/F_{13}-POSS concentration (0.1 wt%), the decline of surface tension is less prominent compared to that for Ph_7/F_{13}-POSS alone at the same concentration (Fig. 2d). In contrast, at higher concentration (0.3–0.5 wt%), at the overall behavior is comparable to that observed for Ph_7/F_{13}-POSS alone. This observation points out a competition between Ph_7/F_{13}-POSS and Pd@SiNP_F_{17} for the gas–liquid interface which is similar to that observed in aqueous particles/surfactant systems.[40]

Fig. 4d shows a schematic representation of the Ph_7/F_{13}-POSS and Pd@SiNP_F_{17} systems. Pd@SiNP_F_{17} particles are predominantly wetted by the gas phase (contact angle >90°) and are therefore badly dispersed in the liquid, resulting in no foam formation. When a small amount of Ph_7/F_{13}-POSS nanoparticles is added, they adsorb on Pd@SiNP_F_{17}, embedding the fluorinated chains while exposing phenyl groups to the liquid phase (red curve in Fig. 3a). This results in better particle dispersion. At an optimal Ph_7/F_{13}-POSS/Pd@SiNP_F_{17} ratio, the interfacial contact angle falls into the "foaming window", resulting in stable foam formation (green curve in Fig. 3a). Further increase of the Ph_7/F_{13}-POSS concentration favors Ph_7/F_{13}-POSS adsorption at the gas–liquid interface, whereas Pd@SiNP_F_{17} particles are pushed into the bulk liquid. Foamability continues to increase, while foam stability drops drastically (violet curve in Fig. 3a).

Ph_7/F_{13}-POSS can also be applied to phase inversion. A BnOH marble can be stabilized using solely Pd@SiNP_F_{17} particles, while a mixture of these particles with Ph_7/F_{13}-POSS allows foam generation. Ph_7/F_{13}-POSS and Pd@SiNP_F_{17} particles can be separated and isolated from the mixture by washing with THF (see more details in Section 2.5). Then, after drying, Pd@SiNP_F_{17} can be again used for marble generation.

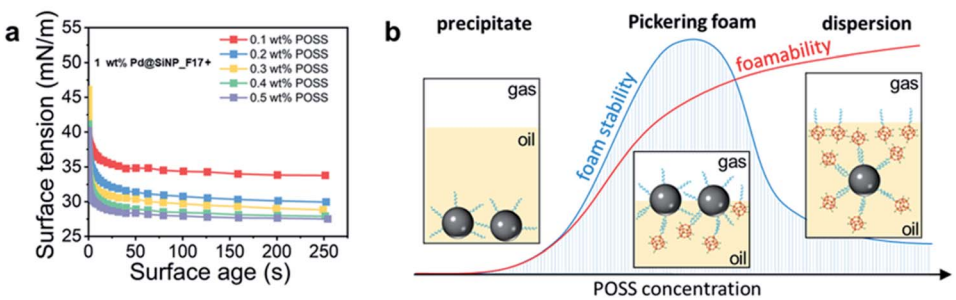

Fig. 4 (a) Dynamic surface tension of benzyl alcohol at 1 wt% Pd@ SiNP_F_{17} and variable Ph_7/F_{13}-POSS concentration. (b) Schematic representation of the synergy between Ph_7/F_{13}-POSS and Pd@SiNP_F_{17} particles.

2.4. Catalysis in benzyl alcohol foams

With these results in hand, we explored the catalytic properties of Pd@SiNP_F_{17} and Ph_7/F_{13}-POSS particle mixtures in the aerobic oxidation of pure benzyl alcohol (BnOH) at 80 °C in the presence of foam. This reaction has been explored in previous studies over transition metal catalysts showing high selectivity to benzaldehyde by avoiding autooxidation.[41,42] In these tests, we kept the Pd@SiNP_F_{17} concentration fixed at 2 wt% while varying the Ph_7/F_{13}-POSS concentration (Fig. 5a). Without Ph_7/F_{13}-POSS, the benzaldehyde (BAH) yield is only 12% after 2 h, while it increases to 90% after addition of 0.1 wt% Ph_7/F_{13}-POSS. This is attributed to a better dispersion of Pd@SiNP_F_{17} particles along with foam generation and transfer of catalytic particles from the bulk to the gas–liquid interface (Fig. 5c and S15†). Increasing the Ph_7/F_{13}-POSS concentration to 0.3–1.0 wt% results in a lower BAH yield due to foam instability (Fig. 5c and S16†). Meanwhile, the interface is mainly populated by Ph_7/F_{13}-POSS, while catalytic Pd@SiNP_F_{17} particles are pushed into the bulk BnOH. A similar reaction pattern is observed at higher Pd@SiNP_F_{17} concentration and a fixed Ph_7/F_{13}-POSS concentration of 0.1 wt% (Fig. 5b). The highest BAH yield (85%) is achieved at 2 wt% Pd@SiNP_F_{17}, while the highest turnover number (TON) at 2 h (10 700 mol mol^{-1}) is obtained with 1 wt% Pd@SiNP_F_{17}. The BAH yield decreases at the highest Pd@SiNP_F_{17} concentration (4 wt%), encompassing the genesis of very stable foams. As a result, the 'armored' gas–liquid interface is expected to show lower permeability and in turn poorer O_2 renewal during the reaction.[43]

Optical inspection of the foams after reaction stabilized by a combination of Pd@SiNP_F_{17} and Ph_7/F_{13}-POSS particles reveals the formation of bubbles with a size ranging from 50 to 250 μm (Fig. 5d). By decorating Pd@SiNP_F_{17} particles with rhodamine b isothiocyanate groups, preferential particle adsorption is observed at the gas–liquid interface (Fig. 5e), confirming the interfacial location of the catalytic particles during the reaction. Indeed, a brighter layer of fluorescent particles is clearly visualized at the boundary of bubbles.

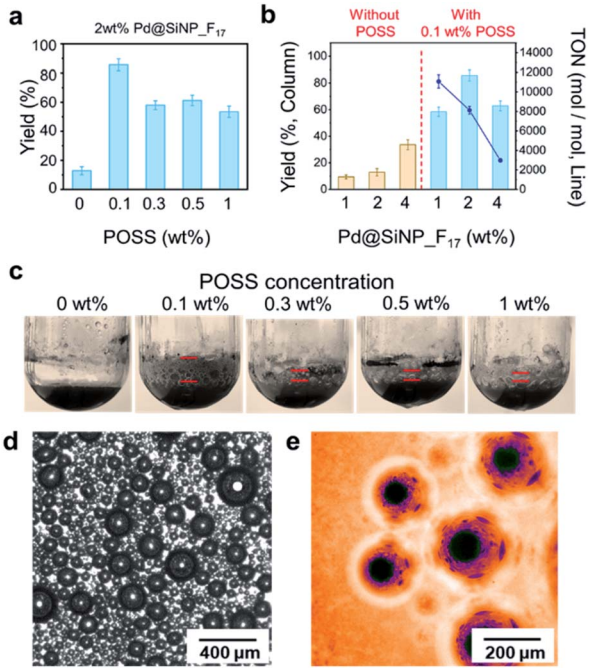

Fig. 5 (a) Aerobic oxidation of BnOH over Pd@SiNP_F_{17} at variable Ph_7/F_{13}-POSS concentration. Reaction conditions: 1.5 mL BnOH, O_2 flow [10 mL(STP) per min], 2 wt% Pd@SiNP_ F_{17}, 1500 rpm, 80 °C, 2 h. (b) Aerobic oxidation of BnOH over Pd@SiNP_F_{17} at variable Pd@SiNP_F_{17} concentration. Reaction conditions: 1.5 mL BnOH, O_2 flow [10 mL(STP) per min], 0.1 wt% Ph_7/F_{13}-POSS, 1500 rpm, 80 °C, 2 h. (c) Optical images of the foam system after the reaction corresponding to (a). (d) Microscopic image of BnOH foam stabilized by 0.1 wt% Ph_7/F_{13}-POSS and 2 wt% Pd@SiNP_F_{17}. (e) Fluorescence microscopy image of BnOH foam stabilized by Ph_7/F_{13}-POSS and rhodamine b isothiocyanate-loaded fluorinated silica particles.

2.5. Particle recycling

The recyclability and reuse of combined 2 wt% Pd@ SiNP_F_{17} and 0.1 wt% Ph_7/F_{13}-POSS particles were studied for the aerobic oxidation of BnOH in seven consecutive runs (see experimental details in the ESI†). After each run, the Pd@SiNP_F_{17} and Ph_7/F_{13}-POSS particle mixture was separated by centrifugation and washed with THF (Fig. 6a). The solid at the bottom of the centrifugation tube was Pd@SiNP_F_{17}, while Ph_7/F_{13}-POSS remained in the supernatant. Pd@SiNP_F_{17} was further separated by decantation, whereas Ph_7/F_{13}-POSS was recovered after THF evaporation. The Ph_7/F_{13}-POSS nanoparticles were dried at 80 °C for 4 h before further use in the subsequent run after remixing with Pd@SiNP_F_{17}. Overall, the particles can be reused at least seven times without an appreciable loss of catalytic activity and foamability (Fig. 6b). Ph_7/F_{13}-POSS

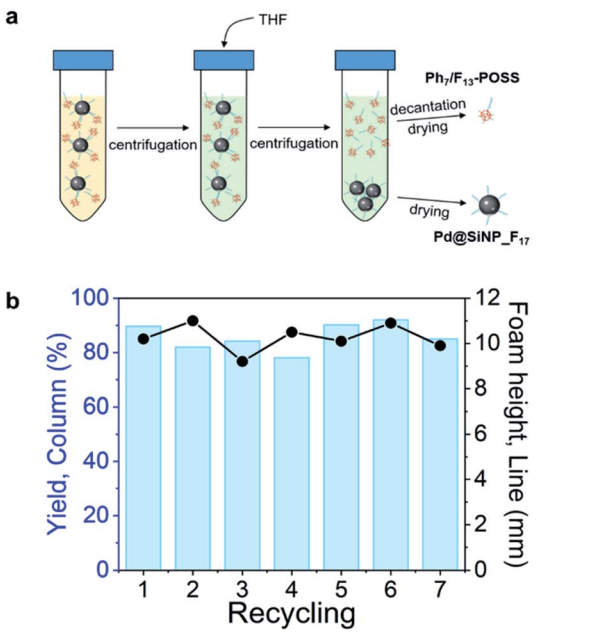

Fig. 6 (a) Schematic representation of the recycling process. (b) Recyclability and reuse of Pd@SiNP_F_{17} and Ph_7/F_{13}-POSS for the aerobic oxidation of BnOH over seven consecutive runs. Reaction conditions: 1.5 mL BnOH, 2 wt% Pd@SiNP_F_{17}, 0.1 wt% Ph_7/F_{13}-POSS, O_2 (flow), 1500 rpm, 80 °C, 2 h.

Table 1 Substrate scope expansion for catalytic tests in an O_2 flow[a]

Reactant	Pd@SiNP_F_{17}/wt%	Ph_7/F_{13}-POSS/wt%	T/°C	t/h	Yield/%
	2	—	100	2	5.6
	2	0.1	100	2	50
	2	—	120	2	30
	2	0.1	120	2	79
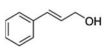	1	—	80	1	12
	1	0.1	80	1	46
	2	0.1	100	0.5	61
	2	0.1	100	1	87

[a] Reaction conditions: 1.5 mL substrate, 1500 rpm, O_2 flow rate [20 mL(STP) per min], and 1 bar O_2.

separation is however limited to liquids with polar groups such as BnOH. For non-polar solvents such as toluene, Ph_7/F_{13}-POSS can hardly be separated by centrifugation due to their good dispersion. No Pd leaching is observed during the reaction, as inferred by ICP-OES.

2.6. Scope of aromatic alcohols

We further examined the generality of aromatic alcohol oxidation in foam systems stabilized by a combination of Pd@SiNP_F_{17} and Ph_7/F_{13}-POSS particles in an O_2 flow (Table 1). The results obtained in the presence of Ph_7/F_{13}-POSS (0.1 wt%) clearly demonstrate higher activity of this system in the oxidation of aromatic alcohols compared to experiments without Ph_7/F_{13}-POSS. For 1-phenylethanol, the acetophenone yield is 50% after 2 h reaction at 100 °C in the foam system containing Ph_7/F_{13}-POSS. This value is about 9 times higher than the yield obtained without Ph_7/F_{13}-POSS. The conversion of methylbenzyl alcohol into the corresponding aldehyde in the presence of foam stabilized by Ph_7/F_{13}-POSS is 79% at 120 °C after 2 h, while the yield is only 30% without Ph_7/F_{13}-POSS. The oxidation of cinnamyl alcohol to cinnamaldehyde shows a yield of 46% at 80 °C after 1 h under foam in the presence of Ph_7/F_{13}-POSS, whereas the yield without Ph_7/F_{13}-POSS is only 12%. Finally, the conversion of benzyl alcohol to benzaldehyde at 100 °C is 61% and 87% after 0.5 and 1 h, respectively.

3. Conclusions

In summary, we prepared oil foams stabilized by a dual particle system combining surface-active catalytic organosilica particles, used as stabilizer, and a novel type of amphiphilic polyhedral oligomeric silsesquioxane (POSS) with surfactant-like properties, used as frother. Both the foamability and foam stability in aromatic solvents are promoted in the presence of a low concentration of POSS, favoring the dispersion of catalytic organosilica particles driven by the interaction between the fluorinated chains of organosilica and POSS particles. As a result, the catalytic activity is drastically enhanced in the presence of POSS with a 9-time increase of the benzaldehyde yield in the oxidation of benzyl alcohol in pure O_2 compared to a catalytic test without POSS. Intermediate foam stability, affording a high gas exchange rate, was required to achieve high catalytic activity. The particles were conveniently recycled with high foamability and the catalytic efficiency was maintained for at least 7 consecutive runs. The dual particle catalytic system was successfully applied to a range of aromatic alcohols, demonstrating the versatility of our approach.

Conflicts of interest

There are no conflicts to declare.

Acknowledgements

This study was funded by the ERC grant Michelangelo (contract number #771586).

Notes and references

1 E. Dickinson, *Curr. Opin. Colloid Interface Sci.*, 2010, **15**, 40–49.
2 R. Farajzadeh, A. Andrianov, R. Krastev, G. J. Hirasaki and W. R. Rossen, *Adv. Colloid Interface Sci.*, 2012, **183**, 1–13.
3 K. A. Matis and P. Mavros, *Sep. Purif. Methods*, 1991, **20**, 163–198.
4 R. Höfer, F. Jost, M. J. Schwuger, R. Scharf, J. Geke, J. Kresse, H. Lingmann, R. Veitenhansel and W. Erwied, *Foams and Foam Control*, VCH, Weinheim, 1988, vol. 11.
5 R. Murakami and A. Bismarck, *Adv. Funct. Mater.*, 2010, **20**, 732–737.
6 J. Huang, F. Cheng, B. P. Binks and H. Yang, *J. Am. Chem. Soc.*, 2015, **137**, 15015–15025.
7 A. L. Fameau, A. Carl, A. Saint-Jalmes and R. Von Klitzing, *ChemPhysChem*, 2015, **16**, 66–75.
8 A. R. Cox, D. L. Aldred and A. B. Russell, *Food Hydrocolloids*, 2009, **23**, 366–376.
9 B. P. Binks and T. S. Horozov, *Angew. Chem., Int. Ed.*, 2005, **44**, 3722–3725.
10 B. P. Binks and H. Shi, *Langmuir*, 2020, **36**, 991–1002.
11 T. N. Hunter, R. J. Pugh, G. V. Franks and G. J. Jameson, *Adv. Colloid Interface Sci.*, 2008, **137**, 57–81.
12 R. Murakami and A. Bismarck, *Adv. Funct. Mater.*, 2010, **20**, 732–737.
13 Y. Han, J. Yang, M. Jung, S. Han, S. Kim and H. S. Jeon, *Langmuir*, 2020, **36**, 10331–10340.
14 A. Maestro, E. Rio, W. Drenckhan, D. Langevin and A. Salonen, *Soft Matter*, 2014, **10**, 6975–6983.
15 L. R. Arriaga, W. Drenckhan, A. Salonen, J. A. Rodrigues, R. Íñiguez-Palomares, E. Rio and D. Langevin, *Soft Matter*, 2012, **8**, 11085–11097.
16 Z. Wang, Y. Li, X. H. Dong, X. Yu, K. Guo, H. Su, K. Yue, C. Wesdemiotis, S. Z. D. Cheng and W. Bin Zhang, *Chem. Sci.*, 2013, **4**, 1345–1352.
17 K. Wu, M. Huang, K. Yue, C. Liu, Z. Lin, H. Liu, W. Zhang, C. H. Hsu, A. C. Shi, W. Bin Zhang and S. Z. D. Cheng, *Macromolecules*, 2014, **47**, 4622–4633.

18 N. Ahmed, H. Fan, P. Dubois, X. Zhang, S. Fahad, T. Aziz and J. Wan, *J. Mater. Chem. A*, 2019, **7**, 21577–21604.
19 L. A. Bivona, O. Fichera, L. Fusaro, F. Giacalone, M. Buaki-Sogo, M. Gruttadauria and C. Aprile, *Catal. Sci. Technol.*, 2015, **5**, 5000–5007.
20 C. H. Lu and F. C. Chang, *ACS Catal.*, 2011, **1**, 481–488.
21 P. Sangtrirutnugul, T. Chaiprasert, W. Hunsiri, T. Jitjaroendee, P. Songkhum, K. Laohhasurayotin, T. Osotchan and V. Ervithayasuporn, *ACS Appl. Mater. Interfaces*, 2017, **9**, 12812–12822.
22 K. Koh, S. Sugiyama, T. Morinaga, K. Ohno, Y. Tsujii, T. Fukuda, M. Yamahiro, T. Iijima, H. Oikawa, K. Watanabe and T. Miyashita, *Macromolecules*, 2005, **38**, 1264–1270.
23 V. Vij, T. S. Haddad, G. R. Yandek, S. M. Ramirez and J. M. Mabry, *Silicon*, 2012, **4**, 267–280.
24 H. Araki and K. Naka, *Macromolecules*, 2011, **44**, 6039–6045.
25 W. Wang, W. Ding, J. Yu, M. Fei and J. Tang, *J. Polym. Res.*, 2012, **19**, 9948.
26 M. Ye, Y. Wu, W. Zhang and R. Yang, *Res. Chem. Intermed.*, 2018, **44**, 4277–4294.
27 S. T. Iacono, A. Vij, W. Grabow, D. W. Smith and J. M. Mabry, *Chem. Commun.*, 2007, 4992–4994.
28 L. Van Ravenstein, W. Ming, R. D. Van de Grampel, R. Van der Linde, G. de With, T. Loontjens, P. C. Thüne and J. W. Niemantsverdriet, *Macromolecules*, 2004, **37**, 408–413.
29 G. D. Chukin and V. I. Malevich, *J. Appl. Spectrosc.*, 1977, **26**, 223–229.
30 S. M. S. Shahabadi, H. Rabiee, S. M. Seyedi, A. Mokhtare and J. A. Brant, *J. Membr. Sci.*, 2017, **537**, 140–150.
31 *Spectroscopy of Aromatic Compounds*, https://chem.libretexts.org/@go/page/31568.
32 D. B. Cordes, P. D. Lickiss and F. Rataboul, *Chem. Rev.*, 2010, **110**, 2081–2173.
33 A. J. Guenthner, K. R. Lamison, L. M. Lubin, T. S. Haddad and J. M. Mabry, *Ind. Eng. Chem. Res.*, 2012, **51**, 12282–12293.
34 W. Zhang, G. Camino and R. Yang, *Prog. Polym. Sci.*, 2017, **67**, 77–125.
35 A. P. Kotula and S. L. Anna, *Soft Matter*, 2012, **8**, 10759–10772.
36 A. Stocco, E. Rio, B. P. Binks and D. Langevin, *Soft Matter*, 2011, **7**, 1260–1267.
37 H. Hou, J. Li, X. Li, J. Forth, J. Yin, X. Jiang, B. A. Helms and T. P. Russell, *Angew. Chem., Int. Ed.*, 2019, **58**, 10142–10147.
38 V. B. Fainerman, V. D. Mys, A. V. Makievski and R. Miller, *J. Colloid Interface Sci.*, 2006, **304**, 222–225.
39 Y. Xue, H. Wang, Y. Zhao, L. Dai, L. Feng, X. Wang and T. Lin, *Adv. Mater.*, 2010, **22**, 4814–4818.
40 R. Pichot, F. Spyropoulos and I. T. Norton, *J. Colloid Interface Sci.*, 2012, **377**, 396–405.
41 M. Sankar, E. Nowicka, E. Carter, D. M. Murphy, D. W. Knight, D. Bethell and G. J. Hutchings, *Nat. Commun.*, 2014, **5**, 1–6.
42 S. Meher and R. K. Rana, *Green Chem.*, 2019, **21**, 2494–2503.
43 S. Zhang, D. Dedovets, A. Feng, K. Wang and M. Pera-Titus, *J. Am. Chem. Soc.*, 2022, **144**(4), 1729–1738.